Complementary bonding analysis of the N–Si interaction in pentacoordinated silicon compounds using quantum crystallography

Malte Fugel, Maksym Ponomarenko, Maxie Hesse, Lorraine Malaspina, Florian Kleemiss, Kunihisa Sugimoto, Alessandro Genoni, Gerd-Volker Röschenthaler, Simon Grabowsky

Complementary bonding analysis of the N–Si interaction in pentacoordinated silicon compounds using quantum crystallography

Malte Fugel[a], Maksym V. Ponomarenko[b], Maxie F. Hesse[a], Lorraine A. Malaspina[a], Florian Kleemiss[a,e], Kunihisa Sugimoto[c], Alessandro Genoni[d], Gerd-Volker Röschenthaler[b], and Simon Grabowsky[a,e,*]

[a]University of Bremen, Department 2: Biology/Chemistry, Institute of Inorganic Chemistry and Crystallography, Leobener Str. 3, 28359 Bremen, Germany.
[b]Jacobs University, Life Sciences & Chemistry, Campus Ring 1, 28759 Bremen, Germany.
[c]JASRI / Diffraction & Scattering Division, 1-1-1 Kouto, Sayo-cho, Sayo-gun, Hyogo 679-5198, Japan.
[d]Université de Lorraine, CNRS, Laboratoire LPCT, 1 Boulevard Arago, 57078 Metz, France.
[e]Current address: University of Bern, Department of Chemistry and Biochemistry, Freiestrasse 3, 3012 Bern, Switzerland. * Corresponding author e-mail address: simon.grabowsky@dcb.unibe.ch

Electronic supplementary information (ESI) available: characterization of compounds, crystallographic details, coordinates of optimized structures. CCDC: 1937643, 1937692, 1937940.

Abstract

The N–Si interaction in two pentacoordinated silicon compounds is investigated based on a *complementary bonding analysis*, which consists of bonding descriptors from real space and orbital space. These are derived from X-ray wavefunction refinements of high-resolution X-ray diffraction data of single crystals and from isolated-molecule theoretical wavefunctions. DELETED The two pentacoordinated compounds only differ in one methylene group, so that the amino substituent is more flexible in one of the structures, hence probing the attractive or repulsive character of the N–Si interaction. All studies suggest weak dative interactions, which do, however, greatly influence the character of the Si–F bond: A strong N–Si interaction results in a weakened Si–F bond, which is quantified in this study experimentally and theoretically.

1 Introduction

In contrast to S_N2 reactions involving carbon electrophiles, where the pentacoordinated species is always a transition state, in silicon chemistry pentacoordination can lead to stable complexes depending on the substitution pattern.[1–3] Therefore, numerous compounds with pentacoordinated silicon atoms are found

in the literature.[4–11] Pentacoordinated silicon compounds in the solid state have, e.g., been used as model systems for the experimental simulation of S_N2 reactions at silicon atoms according to the *structure correlation*[12] philosophy.[13–19] Moreover, N-Si interactions in high-coordinated silicon compounds were subject of experimental charge-density analyses.[20–22] In the present paper, we analyze the bonding situation in two silicon compounds (**1** and **2**), which are depicted in Figure 1, by quantum crystallography.[23,24] In both of these structures, the nitrogen atom is coordinated to the silicon, thus, inflicting a certain degree of pentacoordination. DELETED

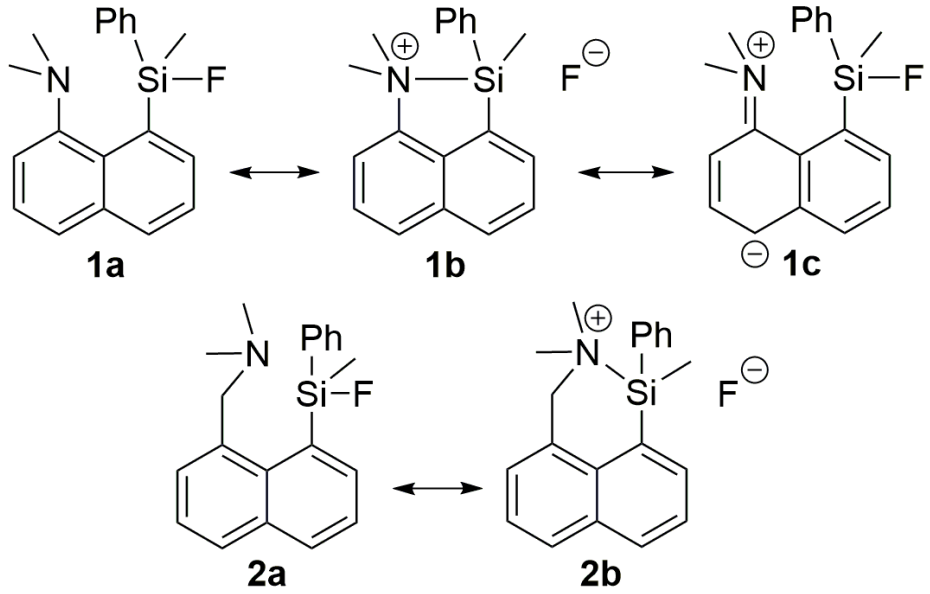

Figure 1: Resonance structures involving the nitrogen lone pair of the Me_2N (**1a-c**) and Me_2NCH_2 (**2a-b**) substituted compounds

The compounds only differ in that compound **2** has a methylene group bridging the amino group and the naphthalene unit. In compound **1**, the N−Si interaction is a peri-interaction, which is enforced by spatial proximity.[25] Hence, the interaction always has an attractive and a repulsive component. For peri-interactions, there are attempts to computationally estimate the ratio of attractive and repulsive energies by isodesmic exchange calculations.[26] Here, we follow a different approach: In compound **2**, free rotation around the methylene group allows the N−Si contact to avoid all enforced interactions, and hence it can serve as a measure of the degree of attractive or repulsive interactions. One of the main objectives of the present paper is to uncover the differences of the N−Si interaction resulting from the additional methylene group in compound **2**. There are three factors differentiating compounds **1** and **2**:

1. The additional methylene group makes the Me_2N group rotationally flexible, so a closer approach of the nitrogen atom towards the silicon atom is possible, or, in turn, avoidance of the contact leading to a longer N−Si distance.

2. The additional methylene group in compound **2** makes one of the substituents bulkier, which causes

a higher steric repulsion compared to compound **1**.

3. Only in the Me_2N substituted compound **1**, the nitrogen lone pair is involved in a resonance with the aromatic system of the naphthalene unit leading to resonance structure **1c** depicted in Figure 1. It is this resonance that causes the reactivity and basicity differences between aniline and benzylamine functional groups.

The N–Si interaction itself may be represented by resonance structures **1b** and **2b** for compounds **1** and **2**, respectively. DELETED In terms of a localized orbital picture, this interaction can be classified as negative hyperconjugation with the nitrogen lone pair acting as a donor orbital and the Si–F localised antibonding orbital acting as an acceptor orbital.[27] Resonance structures with both N–Si and Si–F bonds are not considered, because these hypervalent bonding representations suggest d-orbital participation, which has been shown to be insignificant for bonds involving atoms from the second and third periods.[28–33]

We have discussed previously that a joint application of bond analysis methods from real space (e.g. Quantum Theory of Atoms in Molecules, QTAIM,[34] and the electron localizability indicator, ELI-D[35]) and orbital space (e.g. natural bond orbitals, NBO[27,36]) enhances the information value due to the complementarity of the methods (complementary bonding analysis).[37–39] In the present study, we apply QTAIM, ELI-D, NBO and unconstrained ELMO-VB (extremely localized molecular orbital valence bond)[40,41] analyses to shed light on the N–Si interaction and related bonding properties. The results are produced using X-ray wavefunction refinements (XWR)[42,43] of high-resolution single crystal X-ray diffraction data measured at the synchrotron SPring-8 in Japan. XWR is a novel method from the field of quantum crystallography.[23,24] For a comparison, purely theoretical calculations were performed in addition.

2 Experimental and computational details

2.1 Synthesis

Synthesis of the Me_2N substituted compound (1)

Previously, compound **3** was synthesized by Carré *et al.*[44] However, in this study an alternative route was chosen. 12.52 mL (1 equiv) of *n*-BuLi (2.5 M, in *n*-hexane) were added at 0°C to a solution of *N,N*-dimethylnaphthalen-1-amine (5.36 g, 31.3 mmol) in 35 mL of diethyl ether. The mixture was stirred for 48 h at room temperature. The formed precipitate of the lithiated product was filtered off, and washed with pentane (2 x 20 mL) under argon; then it was dried for 30 min in oil-pump vacuum at room temperature. The solid product was transferred into a 100 mL Schlenk flask, and then 40mL of diethyl ether was added. The mixture was cooled to -60°C, and 4.46 g (23.3 mmol, 1.3 equiv) of $PhSiMeCl_2$ was added through a syringe. The cooling bath was removed after 30 min, and the mixture was stirred for 24 h at room temperature. The formed precipitate was filtered off under argon, and washed with diethyl ether (2 x 5 mL). Diethyl ether was evaporated, and the rest was recrystallized from a saturated hot diethyl ether solution (under argon) giving 1.2 g (20%) of the clean product **3**. The white precipitate, which was

collected after first filtration of the reaction mixture, was mixed with 20 mL of CH_2Cl_2, and the mixture was filtered to remove LiCl. The solvent was evaporated giving 3.6 g (61% yield) of **3**.

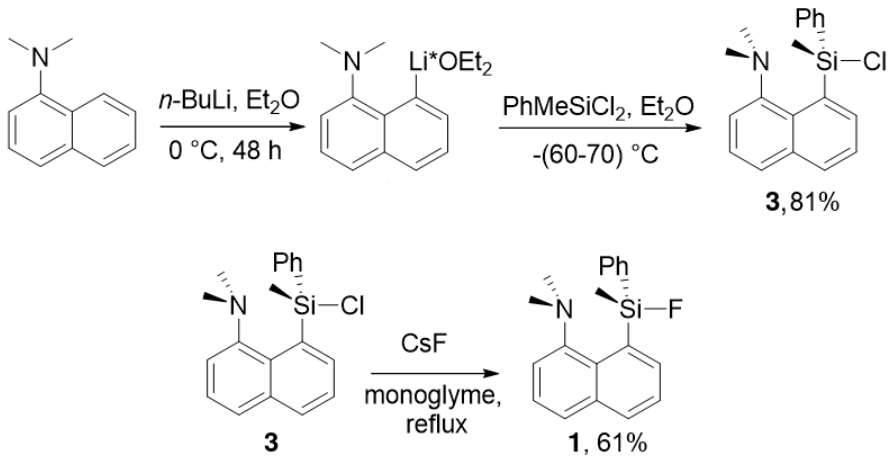

Scheme 1

0.55 g (1.69 mmol) of **3** were added to a mixture of dried CsF (2.56 g, 16.9 mmol) in 20 mL of monoglyme. The mixture was refluxed for 12 h, and cooled to ambient temperature. 20 mL of CH_2Cl_2 was added, and then the reaction mixture was filtered under inert atmosphere. The solvents were removed in oil-pump vacuum. The residue was recrystallized from an *n*-hexane/CH_2Cl_2 mixture giving 0.318 g (61%) of the fluorinated product **1**. Colorless good quality single crystals of **1** were grown by slow evaporation of the solvents under air from an *n*-hexane/CH_2Cl_2 (80/20 v/v) mixture. The fluorinated product **1** becomes darker after two to three weeks of storage at ambient conditions. However, **1** is stable for a long time under inert atmosphere.

Synthesis of the Me_2NCH_2 substituted compound (2)

β-Dimethylaminomethylnaphthalene was prepared according to the literature.[45] 3.10 mL (1 equiv) of *n*-BuLi (2.5 M, in *n*-hexane) was added at 0°C to a solution of β-dimethylaminomethylnaphthalene (1.44 g, 7.77 mmol) in 25 mL of diethyl ether. The mixture was stirred for 24 h at room temperature. The mixture was cooled to 0°C, and left to stay without stirring for a few hours. The dark red supernatant was removed using a syringe, and the solid lithiated amine was dissolved in 50 mL of diethyl ether. The mixture was cooled to -50°C, and 1.98 g (10.9 mmol, 1.4 equiv) of $PhSiMe(OMe)_2$ was added dropwise through a syringe. The cooling bath was removed after 30 min, and the mixture was stirred for 24 h at room temperature. The solvent was evaporated, and the residue was kept for 4 h in oil pump vacuo at 200°C giving 2.24 g (86%) of raw **4**. The product **4** was used in the next step without additional purification. 0.91 g (2.71 mmol) of **4** was diluted in 15 mL of *n*-hexane. The solution was cooled with an ice bath, and BF_3-etherate (0.19 g, 1.34 mmol) was added. The mixture was intensively stirred for 2 h at room temperature. The *n*-hexane phase was removed into another 50 mL Schlenk flask by a syringe. The solid residue was washed with hot *n*-hexane (3 x 5mL). All *n*-hexane fractions were combined in the

Schlenk flask containing the *n*-hexane phase collected from the reaction mixture. The solvent was removed in oil pump vacuo. The white solid obtained was recrystallized three times from a hot saturated solution in *n*-hexane in inert atmosphere giving 0.40 g (48%) of **2**.

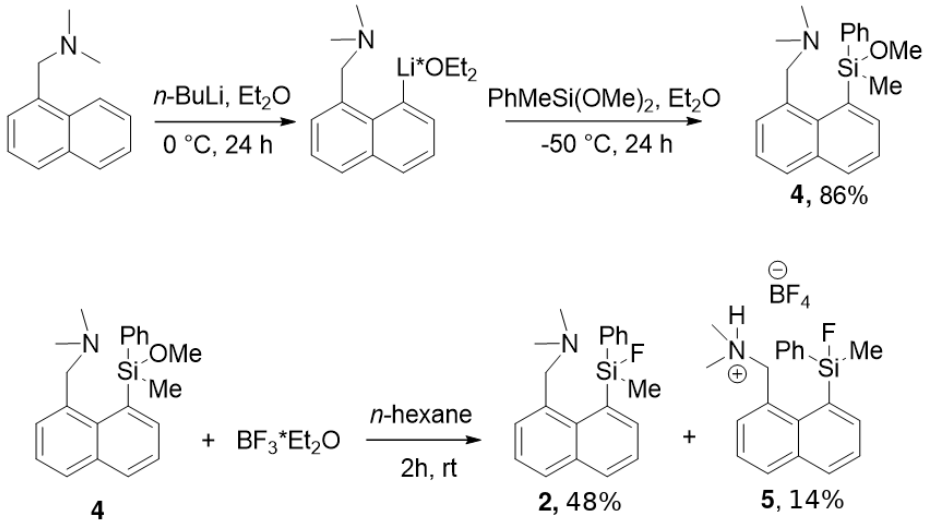

Scheme 2

The slightly yellow residue left in the reaction flask after washing with *n*-hexane was dissolved in a small amount of CH_2Cl_2 (ca. 2 mL). 10 mL of *n*-hexane was carefully layered on top of the CH_2Cl_2 solution. During the solvents diffusion at room temperature white crystals of **5** were formed. The solvents were removed using a syringe, and the product **5** was recrystallized twice in the same manner from a fresh CH_2Cl_2/*n*-hexane mixture giving 0.156 g (14%) of **5**.

^{1}H-, ^{1}3C-, ^{19}F-, ^{29}Si-NMR and high-resolution mass spectrometry data of all synthesized compounds are found in the supporting information.

2.2 Quantum crystallography

Single crystals were obtained from these compounds as explained in the preceding section. High-resolution X-ray diffraction experiments were carried out. For compound **1**, the X-ray diffraction experiment was performed at the synchrotron SPring-8 (Hyogo, Japan) at a temperature of 20 K. For compound **2**, the X-ray diffraction data set was obtained from an in-house measurement with a Bruker D8 Venture at 100 K. Crystallographic information of these structures is given in Table 1. This table also contains the crystallographic information of compound **5**, for which a measurement was performed at SPring8.

After a structure refinement with spherical structure factors (independent atom model), an X-ray wavefunction refinement (XWR) was carried out for compounds **1** and **2**.[42] The first step of an XWR consists of a Hirshfeld atom refinement (HAR) which corresponds to a structure refinement with tailor-made aspherical structure factors obtained from an *ab initio* wavefunction (level of theory: HF/def2-TZVP) by application of Hirshfeld's stockholder partitioning scheme.[46,47] Cluster point charges and dipoles in a

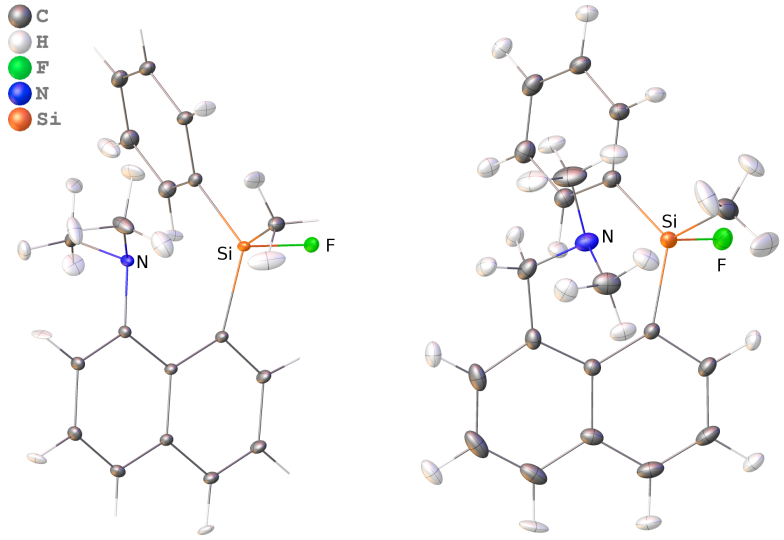

1 **2**

Figure 2: Molecular structures of the Me_2N substituted (left, **1**, only one out of two symmetry-independent molecules is shown) and Me_2NCH_2 substituted (right, **2**) compounds after HAR (ellipsoids are shown at a probability of 50%). Free refinement of hydrogen anisotropic displacement parameters sometimes leads to non-positive definite values (here seen for **1**), but the C−H distances are most accurate nontheless. A detailed discussion about this is found in the literature.[42,48–50]

radius of $r = 8$ Å were used to mimic the crystal environment. The refined crystal structures are shown in Figure 2. There are two molecules in the asymmetric unit of the Me_2N substituted compound **1**. Therefore, properties from both units are given in the following.

In the second step, a wavefunction was fitted to the experimental diffraction data using the same level of theory (X-ray constrained wavefunction fitting, XCW).[51] Crystallographic details for compounds **1** and **2**, as well as for compound **5**, can be obtained from the Cambridge Structural Database numbers listed in Table 1.

Geometry optimizations of the two isolated molecules (**1** and **2**) were carried out with Gaussian 09 at the B3LYP/aug-cc-pVTZ level of theory and application of a dispersion correction (GD3BJ). Frequency analyses were performed to make sure that the optimized structures correspond to minima on the potential energy surfaces.

The X-ray constrained wavefunctions as well as wavefunctions obtained from the geometry optimizations were analyzed with a variety of methods to investigate the bonding situation in these compounds. The NBO analysis was performed with NBO 6.0,[52] and for the QTAIM analysis AIMall[53] was applied. The ELI-D analysis was performed with Dgrid 5.0.[54]

Table 1: Crystallographic information and refinement statistics.

	Me_2N, **1** SPring8	Me_2NCH_2, **2** Home	Me_2NCH_2 (protonated), **5** SPring8
Empirical formula	$C_{19}H_{20}FNSi$	$C_{20}H_{22}FNSi$	$C_{20}H_{23}FNSi^+$ BF_4^-
Space group	P2(1)2(1)2(1)	P2(1)/c	Pn
Crystal system	Orthorhombic	Monoclinic	Monoclinic
a /Å	9.5986(19)	7.5718(3)	13.131(3)
b /Å	11.430(2)	17.2362(6)	7.7980(16)
c /Å	29.056(6)	13.0930(5)	21.291(4)
α /°	90	90	90
β /°	90	95.9760(10)	99.58(3)
γ /°	90	90	90
wavelength /Å	0.4133	0.71073	0.4015
T /K	25(2)	100(2)	20(2)
Crystal dimensions /μm^3	80x60x50	137x179x212	250x180x130
$\sin(\theta)/\lambda_{max}$ /Å^{-1}	0.83	0.91	1.11
R_{int}	0.0304	0.0439	0.0435
N_{meas}, N_{uniq}	71871, 15418	183013, 10700	134595, 44848
N_{obs} (F >4σ)	15240	8971	34497
Redundancy	4.66	17.1	3.0
Completeness	1.00	1.00	0.99
CCDC no.	1937692	1937643	1937940
After IAM			
R1	0.0344	0.0354	0.0602
wR2	0.0918	0.1082	0.1818
$\Delta\rho_{min/max}$ /eÅ^{-3}	-0.56/0.81	-0.34/0.62	-0.88/1.65
After HAR			
R1	0.0251	0.0231	–
wR2	0.0430	0.0322	–
$\Delta\rho_{min/max}$ /eÅ^{-3}	-0.28/0.37	-0.22/0.17	–
After XWR			
λ_{max}	0.15	0.20	–
R1	0.0244	0.016854	–
wR2	0.0398	0.026609	–
$\Delta\rho_{min/max}$ /eÅ^{-3}	-0.27/0.33	-0.19/0.16	–

3 Results and discussion

The analysis of structural parameters provides first hints regarding the bonding situation in compounds **1** and **2**. Table 2 gives a selection of structural parameters of the refined crystal structures and isolated-molecule optimized structures. The N–Si distances in the crystal structures of both compounds are much shorter than the respective N–Si distances of the structures resulting from isolated-molecule optimization. The reason for this is that the electric field of the crystal causes a charge stabilization, which favors a more ionic fluorine atom and, thus, the weights of resonance forms **1b** and **2b** are more significant in the crystal structure compared to the same resonance forms **1b** and **2b** in the isolated molecule. This coincides with the N–Si distances being shorter and the Si–F bonds being somewhat elongated in the solid state. If a geometry optimization is performed with an implicit water solvation without changing any of the other

input parameters, the N–Si distances in the Me_2N substituted compound **1** and the Me_2NCH_2 substituted compound **2** are 2.677 Å and 2.415 Å, respectively, which are close to the distances obtained in the crystal structures. This means that both the electric field imposed by the neighbors in the crystal packing and the neighbors in a water solvation shell can stabilize an ionic bonding situation, thus enhancing the N–Si interaction. Interrelations between the structure of compounds with N-Si dative bonds and the polarity of the surrounding medium have been analysed before.[55,56]

The N–Si interaction seems to be stronger in the Me_2NCH_2 substituted compound **2**, which is implied by a shorter N–Si distance. In turn, the Si–F bond in compound **2** is slightly elongated. With respect to the simulation of S_N2 reactions according to references[13–19], the shorter N–Si distance and elongated Si–F bond length in compound **2** could be interpreted as a more advanced progression of the S_N2 pseudo-reaction. Therefore, it is suggested that resonance structure **2b** is more significant than resonance structure **1b**, see discussion below. At the transition complex (an intermediate state) of an S_N2 reaction, the Si–F bond is oriented approximately 90° to the axial substituents.[1] In fact, the average of these angles is closer to a value of 90° in compound **2**, see Table 2. This is another indication that the Me_2NCH_2 substituted compound **2** is closer to a transition complex than the Me_2N substituted compound **1**, but since all R–Si–F angles exceed a value of 90°, a transition complex is not yet achieved. For compound **2**, the N–Si–F angle is close to 180°. For compound **1**, on the other hand, the N–Si–F angle is below 180°.

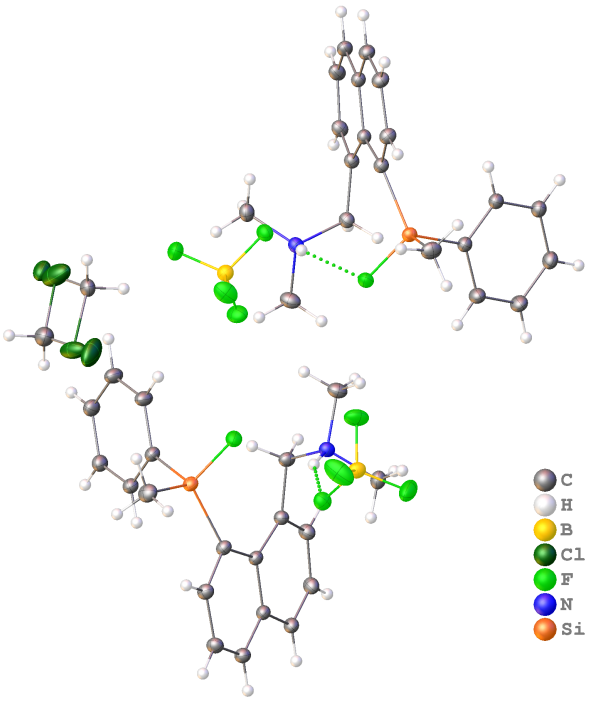

Figure 3: Molecular structures of compound **5** with two symmetry-independent $C_{20}H_{23}FNSi^+$ BF_4^- units after *IAM*; disorder in solvent dichloromethane, anisotropic displacement parameters displayed at 50% probability.

Figure 3 shows the crystal structure of compound **5** after a refinement based on the IAM. There are

two $C_{20}H_{23}FNSi^+$ BF_4^- units in the asymmetric unit of the crystal structure. The compounds in the structure are the protonated form of the Me_2NCH_2 substituted compound **2**. The protonated nitrogen atom can no longer serve as a lone pair donor in the hyperconjugative interaction between the nitrogen lone pair and the Si−F localised antibonding orbital. Instead, an intramolecular hydrogen bond between the fluorine atom and the N−H bond is obtained for one of the symmetry independent units; for the other unit, there is an intermolecular N−H···F hydrogen bond. Consequently, the nitrogen, silicon and fluorine atoms are no longer located on a straight line, but span angles of 45.40° and 44.75°. The N−Si distance is r(N−Si) = 3.669 Å and 3.683 Å, which demonstrates the high degree of freedom of the N−Si distance despite the naphthyl scaffold.

Table 2: Structural parameters from the geometry optimizations and HAR: The N-Si bond length (r(N-Si) in Å), the Si-F bond length (r(Si-F) in Å), the N-Si-F angle (α(N-Si-F) in Å) and the average R-Si-F angle ($<\alpha$(R-Si-F)> in °). The uncertainty of $<\alpha$(R−Si−F)> was derived from the standard deviation of the three R−Si−F angles.

	Me_2N, **1**			Me_2NCH_2, **2**	
	opt.	HAR		opt.	HAR
r(N-Si)	2.7535	2.6593(8)	2.7103(8)	2.6478	2.4527(3)
r(Si-F)	1.6379	1.6442(7)	1.6426(7)	1.6511	1.6662(2)
$<\alpha$(R-Si-F)>	101.7(26)	100.2(16)	99.3(8)	98.0(8)	95.5(8)
α(N-Si-F)	172.79	171.62(3)	173.02(3)	179.00	178.36(1)

A natural bond orbital (NBO) analysis can provide both a qualitative and quantitative description of the bonding situation based on a localized orbital point of view. The N−Si interaction can be linked to the interaction of the nitrogen lone pair NBO (donor orbital) and the Si−F localised antibonding orbital as acceptor orbital, that is, negative hyperconjugation. Figure 4 depicts the interacting orbitals for both compounds **1** and **2**. Delocalization energies, which are given inside Figure 4 for the optimized geometries[1], provide a measure of the strength of these interactions based on the second order perturbation theory. These values reveal that the N−Si interaction is more pronounced in the Me_2NCH_2 substituted compound **2** by ≈8 kJ/mol. Figure 4 also shows the interaction of the nitrogen lone pair NBO with a C−C localised antibonding orbital of the naphthalene unit in the Me_2N substituted compound **1**, which can be attributed to resonance structure **1c**. Based on the delocalization energy, this interaction is even more significant than the N−Si hyperconjugative interactions.

The population of the Si−F localised antibonding orbitals (see Table 3) is another measure of the strength of the N−Si interaction. The population of the antibonding orbital is the highest in the Me_2NCH_2 substituted compound **2** indicating stronger hyperconjugative interactions than those in the Me_2N substituted compound **1**. However, the populations are quite small because they only account for one specific hyperconjugative interaction, but not for all electrons withdrawn from the nitrogen lone pair orbitals,

[1]The calculation of delocalization energies from XWR is not yet applicable.

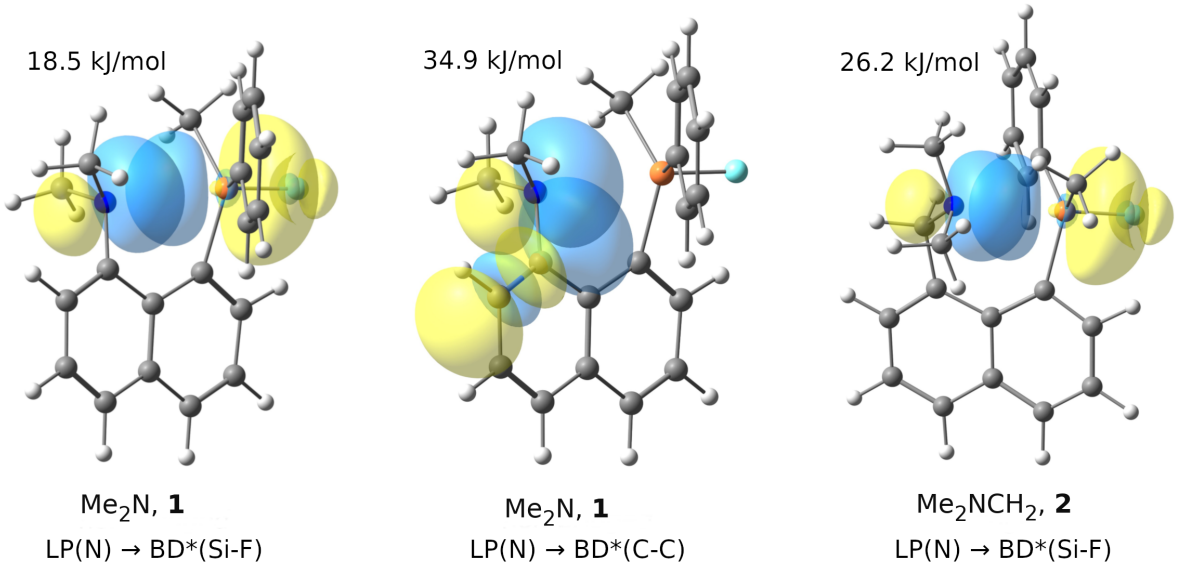

Figure 4: Representation of the natural bond orbitals involved in the LP(N)→BD*(Si−F) and LP(N)→BD*(C−C) negative hyperconjugative interactions with the corresponding delocalization energies (E2) from theory based on the optimized geometries.

Table 3: Bonding properties from NBO (populations of the nitrogen lone pair and Si−F localised antibonding orbital (n(LP(N)) and n(BD*(Si-F)) in e) and NRT weights of the N-Si$^+$ F$^-$ resonance structure (w_{NRT}) in %)

	Me_2N, **1**			Me_2NCH_2, **2**	
	opt.	XWR		opt.	XWR
n(LP(N))	1.821	1.863	1.867	1.818	1.817
n(BD*(Si-F))	0.064	0.066	0.063	0.075	0.094
w_{NRT}(N-Si$^+$ F$^-$)	3.64	3.20	3.04	4.09	4.89

which are involved in a variety of interactions and are hence further delocalized. Therefore, an analysis of the nitrogen NBO lone pair population in terms of the strength of the N−Si interaction is not applicable; it is always important to compare a variety of alternative methods, which we call a *complementary bonding analysis.*[37]

A more direct access to the resonance structures depicted in Figure 1 is obtained from a local natural resonance theory (NRT) analysis.[57] Resonance structures involving only the nitrogen, silicon and fluorine atoms are calculated and a weight is assigned to them. Table 3 lists the weights of resonance structures **1b** and **2b**, which once again indicates that resonance structure **2b** is more significant than resonance structure **1b**. However, it is shown that the localized resonance structures **1a** and **2a** are most significant with weights far exceeding 90%. The N−Si interaction may therefore be regarded as a dative bond with nitrogen's electron pair largely maintaining its lone pair character.

Table 4: Weights of the resonance structures (see Figure 1) obtained from the ELMO-VB calculations (using the cc-pVDZ basis set) based on optimized and HAR geometries.

	Me_2N, **1**			Me_2NCH_2, **2**	
	opt.	HAR		opt.	HAR
$w_{\text{ELMO-VB}}$(**1a**/**2a**)	0.87	0.85	0.86	0.88	0.82
$w_{\text{ELMO-VB}}$(**1b**/**2b**)	0.08	0.11	0.10	0.12	0.18
$w_{\text{ELMO-VB}}$(**1c**)	0.04	0.04	0.04	–	–

Valence bond (VB) calculations based on extremely localized molecular orbitals (ELMOs) also provide an access to structural weights.[40,41,58] The weights of the ELMO-VB structures depicted in Figure 1 are listed in Table 4. Resonance structures **1a** and **1b** are by far the most significant ones as for NRT, but the respective weights are lower by about 10%. The weight of resonance structure **2b** of compound **2** is higher than the weight of resonance structure **1b** of compound **1**. Here, the ELMO-VB approach shows an even more pronounced difference compared to the weights from NRT. The weight of resonance structure **1c** is ≈4% in compound **1**, which indicates that the N–Si interaction is more significant than the N–C interaction, in contrast to the delocalization energies from NBO.

An analysis based on the Quantum Theory of Atoms in Molecules (QTAIM) provides further insight into the character of the dative N–Si bond as well as the Si–F bond. Figure 5 shows all bond paths obtained for both compounds from theory and XWR. A bond path corresponds to a path of maximum electron density which indicates a bonded interaction.[59–61] The converse argument is not valid: A bonded interaction can be present although a bond path is absent. This was shown, e.g., using N-Si dative interactions.[62,63] In our study, in all cases, the analyses yield an N–Si bond path. However, they differ from bond paths of regular covalent bonds in that they are curved close to the silicon atom (compare to the straight C–C, N–C, Si–C and Si–F bond paths), with the exception of compound **2** from XWR, for which a straight N–Si bond path is obtained. A curved bond path is an indication of a weak interaction. Accordingly, the straight bond path obtained for compound **2** from XWR hints at a stronger N–Si interaction. The character of the N–Si interactions and Si–F bonds can be quantified by examining properties at the N–Si and Si–F bond critical points (bcps, saddle points of the electron density which are intersected by the bond paths), see Table 5.

The value of the electron density at a bond critical point is indicative of the strength of the covalent contribution to the bonded interactions. Once again, the N–Si interactions in the Me_2NCH_2 substituted compound **2** are revealed to be the strongest ones. This is in agreement with the value of the total energy density at the N–Si bond critical points, which is more negative for compound **2** suggesting a higher degree of covalency.[65–67] However, the magnitudes of these values imply relatively weak interactions in comparison to values taken from the literature for a standard covalent N-Si bond[22,64] and for a dative N-Si bond in a hexacoordinated silicon compound,[20] also collected in Table 5. In turn, the electron density at the Si–F bond critical points of the Me_2N substituted compound **1** is higher than the one of compound **2**

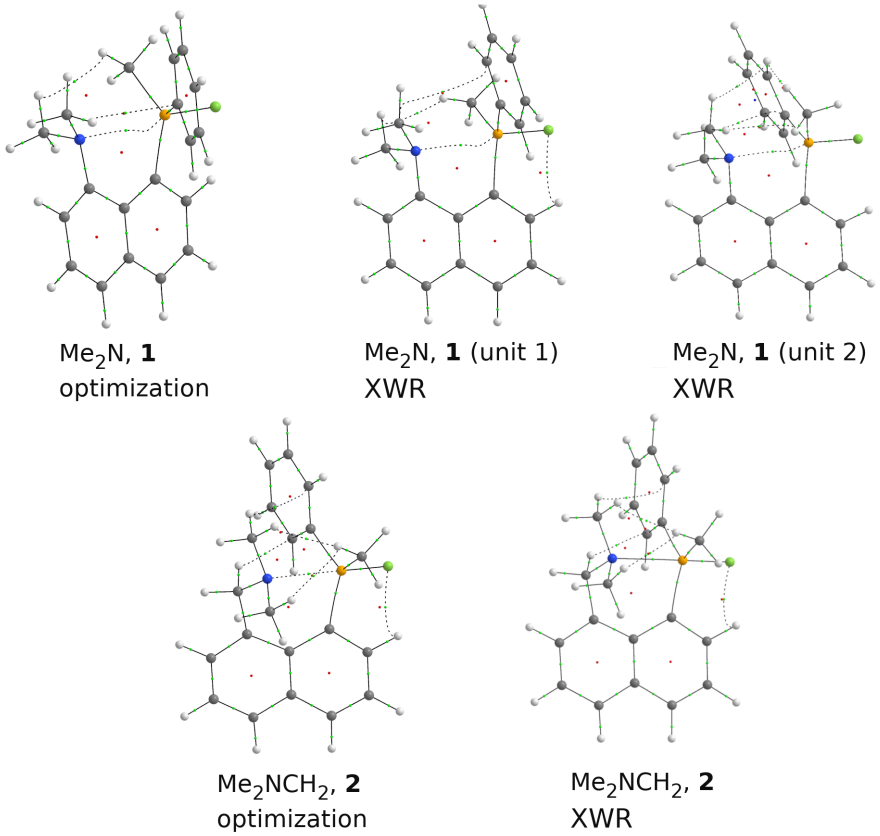

Figure 5: QTAIM bond paths obtained from theory and XWR (a dashed line corresponds to a weak interaction as defined in the software AIMAll by the value of the electron density at the bond critical point), red speres = bond critical points, green spheres = ring critical points

Table 5: N-Si and Si-F bond critical point properties from QTAIM for both compounds **1** and **2**, compared to a standard covalent N-Si bond in $[HN(SiMe_2)]_4$ [22,64] and to a dative N-Si bond in the hexacoordinated silicon compound $F_2Si[O(CPh)N(NMe_2)]_2$ [20]: Electron density (ρ_{bcp} in e·Å^{-3}) and total energy density (H_{bcp} in Hartree·Å^{-3}). MM = multipole model.

	Me_2N, **1**			Me_2NCH_2, **2**		$[HN(SiMe_2)]_4$,[22,64]		$F_2Si[O(CPh)N(NMe_2)]_2$,[20]	
	opt.	XWR		opt.	XWR	opt.	MM	opt.	MM
ρ_{bcp}(N-Si)	0.140	0.166	0.153	0.168	0.240	N/A	0.98(av.)	0.565	0.501
H_{bcp}(N-Si)	-0.0014	-0.0033	-0.0023	-0.0038	-0.0114	N/A	-0.086(av.)	-0.049	-0.011
ρ_{bcp}(Si-F)	0.847	0.844	0.849	0.821	0.769	N/A	N/A	0.769	1.015
H_{bcp}(Si-F)	-0.0376	-0.0390	-0.0395	-0.0365	-0.0275	N/A	N/A	-0.039	-0.076

indicating the Si−F bonds to be weaker in compound **2**. Consequently, a stronger N−Si interaction comes with a weakened Si−F bond. This is in agreement with the previous analyses which found that the Si−F bonds are elongated, and that the Si−F localised antibonding orbitals are more populated in compound

2.

A topological analysis of the electron localizability indicator (ELI-D) yields basins which can be linked to features of Lewis structures, such as bonds and lone pairs.[35] Figure 6 depicts ELI-D iso-surfaces revealing bonding and lone pair domains in both compounds. For the Me_2N substituted compound **1** and the optimized structure of the Me_2NCH_2 substituted compound **2**, a nitrogen lone pair basin is obtained. Compound **1** from XWR, on the other hand, gives an N–Si bonding basin instead. Whether a lone pair or bonding basin is obtained depends on the number of neighboring core basins: The nitrogen lone pair is only in contact with a nitrogen core basin (monosynaptic), while the N–Si bond is in contact with the nitrogen and silicon core basins (disynaptic).[35] Both types of basins are located in close proximity to the nitrogen core basin and they have a similar appearance. However, the lone pair basin of compound **2** already shows a hump directed towards the silicon atom, which indicates that it is very close to forming a disynaptic bond basin (Figure 6).

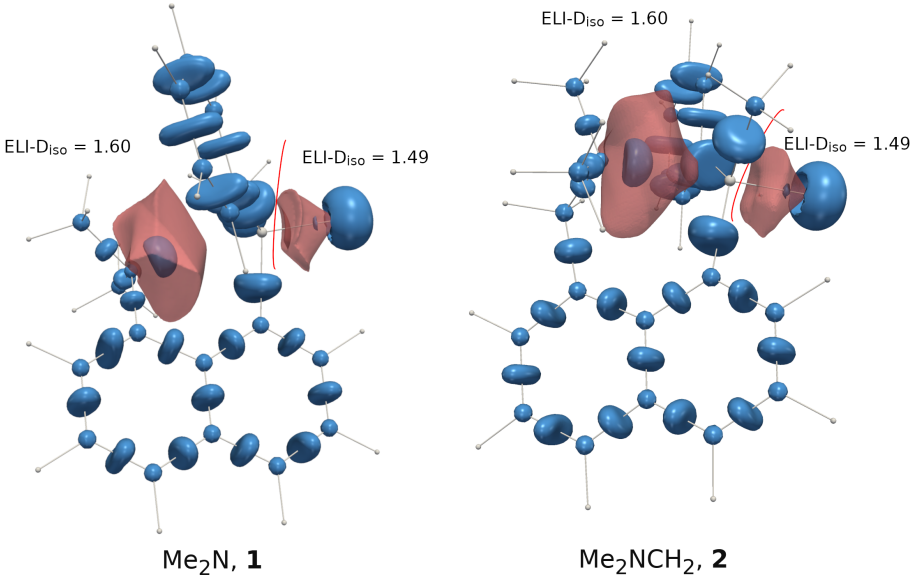

Figure 6: Iso-surfaces (blue) of the ELI-D showing bonding and lone pair domains and topological ELI-D basins (red) of the nitrogen lone pair and Si–F bonds from theory. For compound **2** from XWR, the nitrogen lone pair basin turns into an N–Si bond basin, however, the representation looks virtually indentical (not shown).

An integration of the electron density inside these basins yields electron populations of the lone pair and bonding basins, which are listed in Table 6 for the nitrogen lone pairs as well as N–Si and Si–F bonding basins. The populations of the Si–F bonds are far below two electrons, according to which the covalent bond order of the Si–F bonds is below a value of 1.0. This is caused by the fact that the lone pair basins of the fluorine atom absorb a large amount of the bonding electron density. This is a common feature of the ELI-D observed for bonds involving electronegative and lone pair rich atoms.[37] The Si–F

Table 6: ELI-D electron populations (n in e) of the disynaptic Si-F and N-Si basins and the monosynaptic N basin

	Me_2N, **1**			Me_2NCH_2, **2**	
	opt.	XWR		opt.	XWR
n(Si-F)	0.936	1.4311	1.356	0.914	0.556
n(N-Si)	–	–	–	–	2.148
n(LP(N))	2.131	2.202	2.100	2.185	–
n(LP(F))	6.829	6.359	6.441	6.846	7.223

bonding populations are similar for the geometry optimized compounds **1** and **2**, with the population of compound **2** being only slightly lower. The Si−F population of compound **2** from XWR, on the other hand, is significantly lower than the one of compound **1** from XWR suggesting a more ionic fluorine atom. Accordingly, the lone pair populations of compound **2** from XWR are closer to eight electrons. Directly measuring the strength of the N−Si interaction through nitrogen lone pair populations is not feasible. In fact, the population of the N−Si bonding basin of compound **2** from XWR is similar to those of the nitrogen lone pair basins, which once again indicates a similar character.

Finally, we study two types of bond orders – the NLMO/NPA bond order (from the NBO analysis)[27] and the delocalization index (DI, from the QTAIM)[68] – which measure the number of electron pairs shared between two atoms. For homopolar single bonds, a bond order of approximately one is expected. Bond polarization reduces the number of shared electrons and, thus, bond orders of below one are obtained. The N−Si bond orders are far below one for both compounds, which is in line with its dative bond character. All NLMO/NPA bond orders are lower than the delocalization indices, but both bond orders give the same trend. The N−Si bond orders of compound **2** are higher than those of compound **1**, which is caused by a stronger N−Si interaction in **2**. From the aforementioned bonding descriptors, lower Si−F bond orders are expected for compound **2**. However, this trend is only observed when comparing the bond orders of the geometry optimized structures among each other. For the bond orders derived from XWR, an opposite trend is retrieved. The fact that all Si−F bond orders are much smaller than one reflects the highly polarized character of the Si−F bonds.

Table 7: NLMO/NPA bond orders and delocalization index (DI) of the N−Si and Si−F bonds

	Me_2N, **1**			Me_2NCH_2, **2**	
	opt.	XWR		opt.	XWR
$BO_{NLMO/NPA}$(N-Si)	0.038	0.044	0.043	0.050	0.092
$BO_{NLMO/NPA}$(Si-F)	0.292	0.260	0.272	0.278	0.255
DI(N-Si)	0.056	0.058	0.058	0.082	0.114
DI(Si-F)	0.337	0.255	0.253	0.324	0.259

4 Conclusions

The N–Si peri-interaction was investigated in the two naphthyl-based pentacoordinated silicon compounds depicted in Figure 1. An investigation of structural parameters confirms that the N–Si interaction is the strongest in the Me_2NCH_2 substituted compound **2**. This is caused by the higher conformational flexibility of the nitrogen atom due to the insertion of the additional bridging methylene group and the absence of interactions involving the nitrogen lone pair and naphthalene unit. Hence, attractive N–Si interactions are more important than steric repulsion in the peri-contact. At the same time, longer Si–F bond lengths are obtained for compound **2** which imply weaker Si–F bonds. Although the analysis of structural parameters already allows for these conclusions, the nature of the N–Si interaction remains uncertain. This is remedied by a *complementary bonding analysis* which comprises NBO, NRT, QTAIM, ELI-D and unconstrained ELMO-VB analyses. Apart from confirming the conclusions drawn from the analysis of structural parameters, a *complementary bonding analysis* enables a characterization of the N–Si interaction leading to the following remarks:

1. The NBO analysis attributes the N–Si interaction to a negative hyperconjugation involving the nitrogen lone pair as a donor orbital and the localised Si–F antibonding orbital as an acceptor orbital.

2. The N–Si interaction is weak and can be regarded as a dative bond – the nitrogen lone pair character is largely maintained.

3. The Si–F bond is highly polarized. The degree of Si–F bond polarization is higher for stronger N–Si interactions.

DELETED In this study, the difference in the strength of the N–Si interaction between compounds**1** and **2** is caused by the additional methylene group in **2**, but, alternatively, the N–Si interaction could be tuned by exchanging the fluorine atom with a variety of different substituents. In a forthcoming study, we present such a systematic array of pentacoordinated silicon compounds, in which we go beyond Bürgi's structure correlation attempting to find correlations with properties obtained from a *complementary bonding analysis*.

Conflicts of interest

The authors declare no conflicts.

Acknowledgements

S.G. thanks the German Research Foundation (Deutsche Forschungsgemeinschaft, DFG) for funding within the Emmy Noether project GR 4451/1-1.

References

[1] A. P. Bento, M. Solà and F. M. Bickelhaupt, *J. Comput. Chem.*, 2005, **26**, 1497–1504.

[2] L. H. Sommer, *Stereochemistry, mechanism and silicon*, McGraw-Hill, 1965.

[3] A. P. Bento and F. M. Bickelhaupt, *J. Org. Chem.*, 2007, **72**, 2201–2207.

[4] C. Chuit, R. J. P. Corriu, C. Reye and J. C. Young, *Chem. Rev.*, 1993, **93**, 1371–1448.

[5] C. Breliere, F. Carre, R. J. Corriu, M. Poirier and G. Royo, *Organometallics*, 1986, **5**, 388–390.

[6] J. M. Anglada, C. Bo, J. M. Bofill, R. Crehuet and J. M. Poblet, *Organometallics*, 1999, **18**, 5584–5593.

[7] R. J. Corriu, A. Kpoton, M. Poirier, G. Royo, A. de Saxcé and J. C. Young, *J. Organomet. Chem.*, 1990, **395**, 1–26.

[8] M. S. Gordon, L. P. Davis and L. W. Burggraf, *Chem. Phys. Lett.*, 1989, **163**, 371–374.

[9] R. J. Corriu, A. Kpoton, M. Poirier, G. Royo and J. Y. Corey, *J. Org. Chem.*, 1984, **277**, C25–C30.

[10] D. Kost and I. Kalikhman, *Adv. Organomet. Chem.*, 2004, **50**, 1–107.

[11] D. Kost and I. Kalikhman, *Acc. Chem. Res.*, 2008, **42**, 303–314.

[12] H.-B. Bürgi and J. D. Dunitz, *Structure correlation*, VCH, Weinheim, 2008.

[13] A. R. Bassindale, M. Borbaruah, S. J. Glynn, D. J. Parker and P. G. Taylor, *Perkin Trans.*, 1999, 2099–2109.

[14] M. Sohail, R. Panisch, A. Bowden, A. Bassindale, P. Taylor, A. Korlyukov, D. Arkhipov, L. Male, S. Callear, S. Coles *et al.*, *Dalton Trans.*, 2013, **42**, 10971–10981.

[15] A. Macharashvili, V. Shklover, Y. T. Struchkov, G. Oleneva, E. Kramarova, A. Shipov and Y. I. Baukov, *ChemComm*, 1988, 683–685.

[16] A. R. Bassindale, M. Borbaruah, S. J. Glynn, D. J. Parker and P. G. Taylor, *J. Org. Chem.*, 2000, **606**, 125–131.

[17] A. R. Bassindale, S. J. Glynn, P. G. Taylor, N. Auner and B. Herrschaft, *J. Org. Chem.*, 2001, **619**, 132–140.

[18] A. R. Bassindale, D. J. Parker, P. G. Taylor, N. Auner and B. Herrschaft, *J. Org. Chem.*, 2003, **667**, 66–72.

[19] A. R. Bassindale, D. J. Parker, P. G. Taylor and R. Turtle, *Z. Anorg. Allg. Chem.*, 2009, **635**, 1288–1294.

[20] N. Kocher, J. Henn, B. Gostevskii, D. Kost, I. Kalikhman, B. Engels and D. Stalke, *J. Am. Chem. Soc.*, 2004, **126**, 5563–5568.

[21] D. Stalke, *Struct. Bonding*, 2016, **169**, 57–88.

[22] B. Niepötter and D. Stalke, *Organosilicon Compounds*, Elsevier, 2017, pp. 3–58.

[23] S. Grabowsky, A. Genoni and H.-B. Bürgi, *Chem. Sci.*, 2017, **8**, 4159–4176.

[24] A. Genoni, L. Bučinskỳ, N. Claiser, J. Contreras-García, B. Dittrich, P. M. Dominiak, E. Espinosa, C. Gatti, P. Giannozzi, J.-M. Gillet, D. Jayatilaka, P. Macchi, A. Ø. Madsen, L. Massa, C. F. Matta, K. M. Merz, P. N. H. Nakashima, H. Ott, U. Ryde, K. Schwarz, M. Sierka and S. Grabowsky, *Chem. Eur. J.*, 2018, **24**, 10881–10905.

[25] V. Balasubramaniyan, *Chem. Rev.*, 1966, **66**, 567–641.

[26] E. Hupf, E. Lork, S. Mebs and J. Beckmann, *Organometallics*, 2015, **34**, 3873–3887.

[27] F. Weinhold and C. R. Landis, *Valency and bonding: a natural bond orbital donor-acceptor perspective*, Cambridge University Press, 2005.

[28] W. Kutzelnigg, *Angew. Chem. Int. Ed.*, 1984, **23**, 272–295.

[29] A. E. Reed and F. Weinhold, *J. Am. Chem. Soc.*, 1986, **108**, 3586–3593.

[30] A. E. Reed and P. von Ragué Schleyer, *J. Am. Chem. Soc.*, 1990, **112**, 1434–1445.

[31] M. Fugel, L. A. Malaspina, R. Pal, S. P. Thomas, M. W. Shi, M. A. Spackman, K. Sugimoto and S. Grabowsky, *Chem. Eur. J.*, 2019, **25**, 6523–6532.

[32] M. S. Schmøkel, S. Cenedese, J. Overgaard, M. R. Jørgensen, Y.-S. Chen, C. Gatti, D. Stalke and B. B. Iversen, *Inorg. Chem.*, 2012, **51**, 8607–8616.

[33] D. Stalke, *Chem. Eur. J.*, 2011, **17**, 9264–9278.

[34] R. F. W. Bader, *Chem. Rev.*, 1991, **91**, 893–928.

[35] M. Kohout, *Int. J. Quantum Chem.*, 2004, **97**, 651–658.

[36] F. Weinhold and C. R. Landis, *Chem. Educ. Res. Pract.*, 2001, **2**, 91–104.

[37] M. Fugel, J. Beckmann, D. Jayatilaka, G. V. Gibbs and S. Grabowsky, *Chem. Eur. J.*, 2018, **24**, 6248–6261.

[38] M. Fugel, M. F. Hesse, R. Pal, J. Beckmann, D. Jayatilaka, M. J. Turner, A. Karton, P. Bultinck, G. S. Chandler and S. Grabowsky, *Chem. Eur. J.*, 2018, **24**, 15275–15286.

[39] M. Fugel, F. Kleemiss, L. A. Malaspina, R. Pal, P. R. Spackman, D. Jayatilaka and S. Grabowsky, *Aust. J. Chem.*, 2018, **71**, 227–237.

[40] A. Genoni, *Acta Cryst. A*, 2017, **73**, 312–316.

[41] N. Casati, A. Genoni, B. Meyer, A. Krawczuk and P. Macchi, *Acta Cryst. B*, 2017, **73**, 584–597.

[42] M. Woińska, D. Jayatilaka, B. Dittrich, R. Flaig, P. Luger, K. Woźniak, P. M. Dominiak and S. Grabowsky, *ChemPhysChem*, 2017, **18**, 3334–3351.

[43] S. Grabowsky, P. Luger, J. Buschmann, T. Schneider, T. Schirmeister, A. N. Sobolev and D. Jayatilaka, *Angew. Chem. Int. Ed.*, 2012, **51**, 6776–6779.

[44] F. Carré, R. J. Corriu, A. Kpoton, M. Poirier, G. Royo, J. C. Young and C. Belin, *J. Organomet. Chem.*, 1994, **470**, 43–57.

[45] R. L. Gay and C. R. Hauser, *J. Am. Chem. Soc.*, 1967, **89**, 2297–2303.

[46] D. Jayatilaka and B. Dittrich, *Acta Cryst. A*, 2008, **64**, 383–393.

[47] S. C. Capelli, H.-B. Bürgi, B. Dittrich, S. Grabowsky and D. Jayatilaka, *IUCrJ*, 2014, **1**, 361–379.

[48] L. A. Malaspina, A. J. Edwards, W. Magdalena, D. Jayatilaka, M. J. Turner, J. R. Price, R. Herbst-Irmer, K. Sugimoto, E. Nishibori and S. Grabowsky, *Cryst. Growth Des.*, 2017, **17**, 3812–3825.

[49] B. Dittrich, J. Lübben, S. Mebs, A. Wagner, P. Luger and R. Flaig, *Chem. Eur. J.*, 2017, **23**, 4605–4614.

[50] C. Köhler, J. Lübben, L. Krause, C. Hoffmann, R. Herbst-Irmer and D. Stalke, *Acta Cryst. B*, 2019, **75**, 434–441.

[51] D. Jayatilaka and D. J. Grimwood, *Acta Cryst. A*, 2001, **57**, 76–86.

[52] E. D. Glendening, C. R. Landis and F. Weinhold, *J. Comput. Chem.*, 2013, **34**, 1429–1437.

[53] T. A. Keith, *Version 17*, 2013, **11**, 16.

[54] M. Kohout, *DGrid, version 5.0*, 2016.

[55] M. Hagemann, A. Mix, R. J. Berger, T. Pape and N. W. Mitzel, *Inorg. Chem.*, 2008, **47**, 10554–10564.

[56] M. Hagemann, R. J. Berger, S. A. Hayes, H.-G. Stammler and N. W. Mitzel, *Chem. Eur. J.*, 2008, **14**, 11027–11038.

[57] E. D. Glendening and F. Weinhold, *J. Comput. Chem.*, 1998, **19**, 593–609.

[58] A. Genoni and M. Sironi, *Theor. Chem. Acc.*, 2004, **112**, 254–262.

[59] R. F. W. Bader, *J. Phys. Chem. A*, 1998, **102**, 7314–7323.

[60] R. F. W. Bader, *J. Phys. Chem. A*, 2009, **113**, 10391–10396.

[61] M. von Hopffgarten and G. Frenking, *Chem. Eur. J.*, 2008, **14**, 10227–10231.

[62] N. W. Mitzel, K. Vojinović, R. Fröhlich, T. Foerster, H. E. Robertson, K. B. Borisenko and D. W. Rankin, *J. Am. Chem. Soc.*, 2005, **127**, 13705–13713.

[63] N. W. Mitzel, U. Losehand, A. Wu, D. Cremer and D. W. Rankin, *J. Am. Chem. Soc.*, 2000, **122**, 4471–4482.

[64] N. Kocher, C. Selinka, D. Leusser, D. Kost, I. Kalikhman and D. Stalke, *Z. Anorg. Allg. Chem.*, 2004, **630**, 1777–1793.

[65] G. V. Gibbs, M. A. Spackman, D. Jayatilaka, K. M. Rosso and D. F. Cox, *J. Phys. Chem. A*, 2006, **110**, 12259–12266.

[66] G. V. Gibbs, R. T. Downs, D. F. Cox, N. L. Ross, C. T. Prewitt, K. M. Rosso, T. Lippmann and A. Kirfel, *Z. Kristallogr. Cryst. Mater.*, 2008, **223**, 01–40.

[67] D. Cremer and E. Kraka, *Angew. Chem. Int. Ed.*, 1984, **23**, 627–628.

[68] R. F. Bader, A. Streitwieser, A. Neuhaus, K. E. Laidig and P. Speers, *J. Am. Chem. Soc.*, 1996, **118**, 4959–4965.